JAMES | Journal of Advances in Modeling Earth Systems

RESEARCH ARTICLE
10.1029/2023MS003719

Key Points:

- Cloud-resolving simulations with parameterized moisture convergence support multiple equilibria in precipitation over a wet land surface
- Allowing the surface to dry out can trigger transitions from non-precipitating equilibria back to a precipitating states
- The onset of precipitation is linked to less efficient boundary layer ventilation by large-scale subsidence over a drier surface

Correspondence to:
T. H. Abbott,
tristana@princeton.edu

Citation:
Abbott, T. H., & Cronin, T. W. (2023). Multiple equilibria and soil moisture-precipitation feedbacks in idealized convection-permitting simulations with an open hydrological cycle. *Journal of Advances in Modeling Earth Systems*, *15*, e2023MS003719. https://doi.org/10.1029/2023MS003719

Received 21 MAR 2023
Accepted 26 JUL 2023

Author Contributions:
Conceptualization: Tristan H. Abbott, Timothy W. Cronin
Data curation: Tristan H. Abbott
Formal analysis: Tristan H. Abbott
Funding acquisition: Tristan H. Abbott, Timothy W. Cronin
Investigation: Tristan H. Abbott
Methodology: Tristan H. Abbott, Timothy W. Cronin
Project Administration: Tristan H. Abbott, Timothy W. Cronin
Resources: Timothy W. Cronin
Software: Tristan H. Abbott
Supervision: Timothy W. Cronin
Validation: Tristan H. Abbott
Visualization: Tristan H. Abbott

Multiple Equilibria and Soil Moisture-Precipitation Feedbacks in Idealized Convection-Permitting Simulations With an Open Hydrological Cycle

Tristan H. Abbott[1] **and Timothy W. Cronin**[2]

[1]Program in Atmospheric and Oceanic Sciences, Princeton University, Princeton, NJ, USA, [2]Department of Earth, Atmospheric and Planetary Sciences, MIT, Cambridge, MA, USA

Abstract Soil moisture-precipitation feedbacks are influenced by both small-scale land-atmosphere coupling and large-scale atmospheric circulations, and their sign has important implications for the stability of regional hydroclimate. However, the importance of both local and non-local processes makes it difficult to model soil moisture-precipitation feedbacks with high fidelity, limiting our ability to use models to understand controls on their sign. Here, we address this challenge by exploring a promising but seldom-used approach to studying soil moisture-precipitation feedbacks over tropical land: coupling small-domain convection-permitting simulations to a land-like surface and a parameterization of large-scale dynamics. The large-scale dynamics parameterization, based on the weak temperature gradient (WTG) approximation, is a key component that produces an open hydrological cycle with interactive moisture convergence. We first show that WTG-constrained simulations coupled to a freely-evaporating land surface support both precipitating and non-precipitating equilibria across a wide range of insolation. We then leverage this bistability to probe the influence of soil moisture feedbacks on dry spells by asking whether non-precipitating equilibria remain stable as the underlying surface dries out. We find that surface drying can trigger transitions from dry equilibria back to precipitating equilibria—a negative soil moisture-precipitation feedback—and attribute this transition to increasingly inefficient boundary layer ventilation by the parameterized large-scale circulation. In sensitivity experiments, alternative versions of the WTG scheme modify the parameter space where the negative feedback occurs, but none eliminate it entirely. Our results provide a foundation for leveraging the rich behavior of WTG-constrained simulations to probe controls on soil moisture-precipitation feedbacks over tropical land.

Plain Language Summary Land surfaces constantly lose moisture through evaporation, and without rain will eventually become very dry. A key question for researchers interested in understanding drought is whether a drier land surface makes rain less likely (a "positive feedback" that favors intense drought) or more likely (a "negative feedback" that opposes intense drought). However, these feedbacks are difficult to study using computer models, in part because limited computer power makes it difficult to simulate interactions between land and the atmosphere in sufficient detail without neglecting the effects of large-scale winds. We explore a new solution to this dilemma by describing computer simulations that take a novel approach to simulating feedbacks between rain and surface wetness: we devote most of our computational power to simulating land-atmosphere interactions in great detail over a small region, and represent winds that carry moisture into and out of that region using a simple model most appropriate for the tropics. We show that these simulations can model both rainy and drought-like conditions, and show that surface drying under drought conditions can trigger the return of rain—a negative anti-drought feedback. These results provide a foundation for using a new modeling approach to improve our understanding of controls on drought.

1. Introduction

The sign of soil moisture-precipitation feedbacks has important implications for regional hydroclimate over land. A negative feedback, where low soil moisture promotes precipitation, stabilizes the land-atmosphere system against intense dry spells. In contrast, a positive feedback, where low soil moisture inhibits precipitation, allows dry spells to self-reinforce. That a negative feedback is possible at all is testament to the "openness" of the hydrological cycle over land: on regional scales, moisture for precipitation is provided both locally by evaporation and non-locally by large-scale convergence (Trenberth, 1999). Global models with parameterized convection can explicitly simulate large-scale moisture transport, but the use of convective parameterizations can introduce biases

Writing – original draft: Tristan H. Abbott
Writing – review & editing: Tristan H. Abbott, Timothy W. Cronin

toward overly-positive spatial soil moisture-precipitation feedbacks (Hohenegger et al., 2009; Moon et al., 2019; Taylor et al., 2012, 2013), complicating their use as a tool for understanding soil moisture-precipitation feedbacks. Here, we explore an alternative approach to modeling soil moisture-precipitation feedbacks over tropical land: running small-domain convection-permitting simulations, but with the key addition of a parameterized large-scale circulation that "opens" the hydrological cycle and interacts with processes inside the simulated domain. In contrast to simulations with global models, this approach permits explicit simulation of many of the processes involved in local land-atmosphere coupling and has shown impressive skill in simulations of seasonal changes in Amazonian hydroclimate (Anber, Gentine, et al., 2015). Despite these strengths, however, it is not widely used in work on land-atmosphere interactions and remains an unexplored tool for studies of soil moisture-precipitation feedbacks. Our paper fills this gap by exploring mechanisms that regulate the sign and strength of the soil moisture-precipitation feedback in idealized convection-permitting simulations coupled to a parameterized large-scale circulation. Specifically, we focus both on understanding how the temporal evolution of soil moisture affects the persistence of wet and dry states, and on appraising the robustness of our results to the formulation of our large-scale dynamics parameterization.

Past work provides evidence that, at least in certain situations, coarse-resolution models with parameterized convection tend to simulate overly-positive spatial soil moisture-precipitation feedbacks. In global climate models, afternoon convective rain occurs preferentially over locally-wet soil (Moon et al., 2019; Taylor et al., 2012), consistent with quasi-equilibrium-based predictions of a positive feedback (Eltahir, 1998; Findell & Eltahir, 2003). However, observations indicate that afternoon rain is more common over locally dry soil throughout most of the tropics (Guillod et al., 2015; Moon et al., 2019; Taylor et al., 2012), and simulations with resolved rather than parameterized convection reproduce the observed negative spatial feedback in the Sahel (Taylor et al., 2013). Similarly, coarse-resolution simulations of convective rain during the European summer produce higher rainfall when initialized with higher soil moisture, whereas simulations run at convection-permitting resolution often produce higher rainfall when initialized with lower soil moisture (Hohenegger et al., 2009; Leutwyler et al., 2021).

The ability of convection-permitting models to reproduce observed negative spatial soil moisture-precipitation feedbacks has made them a popular tool for idealized process-oriented modeling studies. Past studies have placed a particular emphasis on understanding links between spatial soil moisture variability, convection, and precipitation, and include work examining the effects of soil moisture heterogeneity on the diurnal growth of cumulus clouds (Rieck et al., 2014), comparing the relative importance of soil moisture anomalies and orography (Imamovic et al., 2017), showing that soil moisture feedbacks are able to overcome self-aggregation feedbacks that favor convection in already-moist regions (Hohenegger & Stevens, 2018), and formulating simple models for the intensity of rain over locally-dry soil (Cioni & Hohenegger, 2018). A consistent finding is that mesoscale (O(100 km)) variations in soil moisture promote precipitation over relatively dry soil through thermally-driven boundary layer circulations that converge moisture evaporated by surrounding wet soil, although one study (Froidevaux et al., 2014) points out that background wind can displace the heaviest rainfall relative to the location of strongest boundary layer convergence.

However, small-domain convection-permitting models poorly represent some features of regional climate over tropical land. Doubly-periodic horizontal boundary conditions, which are easy to implement and widely used, prevent any domain-mean moisture convergence or divergence. As a result, non-zero evaporation must be balanced somewhere by precipitation, and simulating a dry region with suppressed convection requires a domain large enough to also contain a wet region with active convection. Prescribing large-scale ascent or subsidence, and calculating the associated moisture convergence and divergence, permits arbitrarily wet or dry domain-mean conditions, but this is also unrealistic. In the tropics, large-scale vertical motion is tightly coupled to convective heating by dynamical constraints that require weak horizontal temperature gradients (Sobel et al., 2001), and is as much a response to the presence or absence of precipitation as it is a cause of either.

These limitations make it difficult to run experiments that capture the full range of feedbacks between soil moisture, convection, and large-scale moisture transport on domains small enough to allow computationally-cheap exploration of parameter space. In this paper, we explore one approach to overcoming them: by coupling a doubly-periodic convection-permitting model to a parameterization of large-scale circulations based on the weak temperature gradient (WTG) approximation (Sobel et al., 2001). WTG parameterizations operate by defining a reference tropical-mean temperature profile, diagnosing large-scale vertical motion profiles that relax simulated

temperature profiles toward the reference profile, and using large-scale vertical motion profiles to calculate large-scale sources and sinks of energy and moisture. The reference temperature profile can either be taken from observations (as in e.g., Anber, Gentine, et al., 2015) or from a simulation of radiative-convective equilibrium (RCE) that produces a dilute moist adiabat consistent with the equilibrium state of the model (as in e.g., Daleu et al., 2015). When coupled to a convection-permitting model, WTG parameterizations produce an open hydrological cycle with large-scale motion and moisture convergence tightly coupled to explicitly-modeled convection, permitting both precipitating "wet" states where rainfall balances evaporation and moisture convergence, and non-precipitating "dry" states where moisture divergence balances evaporation. We use "WTG simulation" to refer to this class of simulations for the remainder of the paper.

In WTG simulations over ocean, the occurrence of wet and dry steady states is controlled most directly by energy input into the atmospheric column. High surface fluxes, produced by high sea surface temperatures or strong near-surface wind, favor wet states with active convection and large-scale ascent, while low surface fluxes favor dry states with suppressed convection and large-scale subsidence (Anber, Wang, & Sobel, 2015; Raymond & Zeng, 2005; Sentić & Sessions, 2017; Sessions et al., 2016; Sobel & Bretherton, 2000; Wang & Sobel, 2011). Strikingly, the sets of boundary conditions that support wet and dry steady states often intersect, allowing simulations to support multiple equilibria (both precipitating and non-precipitating) with identical boundary conditions (Sessions et al., 2010; Sobel et al., 2007). Multiple equilibria in WTG simulations over ocean are maintained by feedbacks between convection and large-scale vertical motion: active convection favors large-scale ascent that itself promotes convection, while the absence of convection favors large-scale subsidence that further suppresses convection (Sessions et al., 2010; Sobel et al., 2007). Whether WTG-constrained simulations also support multiple equilibria in precipitation over land remains largely unexplored, but assuming they are supported prompts a natural question about soil moisture-precipitation feedbacks: do wet and dry states that are stable with fixed soil moisture remain stable when soil moisture is interactive? This is the specific question our paper targets: we first show that multiple equilibria exist over a land surface that evaporates freely, and then examine whether allowing soil moisture to evolve in time can trigger transitions between precipitating and non-precipitating steady states.

We begin in Section 2 by describing the design of WTG simulations over land, including details about the convection-permitting atmospheric model, large-scale dynamics parameterization, and simple land surface scheme. In Section 3, we demonstrate that WTG simulations with fixed soil moisture, allowing for free evaporation, support both wet and dry steady states across a broad range of values of column energy input. In Section 4, we use these wet and dry equilibria as initial conditions for simulations with interactive soil moisture. Starting from wet equilibria, imbalances between precipitation and evaporation are balanced by runoff, and simulations remain wet. Starting from dry equilibria, however, we find that transient reductions in soil moisture can trigger a transition to a wet equilibrium, and we attribute this negative soil moisture-precipitation feedback to weaker drying of the boundary layer by the parameterized large-scale circulation. We explore the robustness of the negative feedback to changes in the formulation of the large-scale dynamics parameterization in Section 5. The two alternative parameterizations that we test modify the range of values of column energy input over which the negative feedback occurs, but neither eliminate it entirely. Finally, we summarize our results in Section 6 and conclude by discussing prospects for using WTG simulations in future research on land-atmosphere interaction.

2. Simulation Design

We conduct simulations with version 6.11.7 of the System for Atmospheric Modeling (SAM, Khairoutdinov & Randall, 2003). All simulations use a 128×128 km^2 doubly-periodic non-rotating domain with no background flow, a horizontal resolution of 1 km, and a stretched vertical grid with 74 levels. Vertical levels and trace gas concentrations are set following the Radiative-Convective Equilibrium Model Intercomparison Project (RCEMIP) protocol (Wing et al., 2018), and the Rapid Radiative Transfer Model (Mlawer et al., 1997) is used to interactively calculate radiative heating rates. Gravity waves are damped by a sponge layer in the top third of the domain. Microphysics are parameterized using the SAM single-moment parameterization (Khairoutdinov & Randall, 2003), sub-grid-scale turbulence is modeled using a first-order Smagorinsky closure, and surface fluxes of sensible and latent heat are calculated using bulk formulas with aerodynamic resistances calculated based on Monin–Obukhov similarity theory.

We first generate a reference tropical-mean temperature profile by running a 100 day simulation of RCE over a 303 K ocean surface and taking an average over the last 20 days. The RCE simulation has a fixed surface albedo

of 0.07, a surface roughness length of 0.0002 m, and time-independent insolation defined by a solar constant of 551.5 W m^{-2} and a zenith angle of 42.43°, chosen following the RCEMIP protocol (Wing et al., 2018) to match the annual-mean insolation and insolation-weighted zenith angle between the Equator and 20°. This combination of parameters produces a steady-state temperature profile close to a moist adiabat with a shallow subcloud layer and near-surface moist static energy (MSE) of about 343 kJ kg^{-1}, similar to convecting regions of the real-world tropics (Zhang & Fueglistaler, 2020).

We then use the tropical-mean temperature profile as input to a suite of simulations coupled to a land-like interactive surface (Section 2.1) and a parameterization of large-scale circulations based on the WTG approximation (Section 2.2).

2.1. Land-Like Interactive Surface

The interactive surface in our WTG simulations is "land-like" in two critical ways. First, the surface temperature is interactive, which in combination with a low surface heat capacity requires a closed surface energy budget even on diurnal time scales. Second, latent heat fluxes are influenced by soil moisture and shut off completely as soil moisture approaches a prescribed "wilting point."

We keep the surface albedo fixed at 0.07 in WTG simulations. This value, which is low relative to most land surfaces, allows parameter sweeps with varied solar latitude to include some simulations where the energy input into the land-atmosphere system is higher than the real-world tropics, as well as some simulations where it is lower. We increase the surface roughness length in simulations with a land-like surface to a land-like value of 0.035 m. Surface temperature at each gridpoint evolves in time according to

$$C_s \frac{\mathrm{d}T_s}{\mathrm{d}t} = SW + LW^- - LW^+ - LHF - SHF, \tag{1}$$

where C_s is the surface heat capacity (set to the equivalent to 5 cm of water following Cronin et al. (2015)), T_s is surface temperature, t is time, SW and LW^- are net shortwave and downward longwave fluxes at the surface, LW^+ is longwave emission from the surface, and LHF and SHF are turbulent fluxes of latent and sensible heat (defined as positive upwards).

Soil moisture is prescribed in some simulations and prognosed in others. When it is prognosed, it evolves in time according to

$$\rho_w D \frac{\mathrm{d}\phi}{\mathrm{d}t} = P - E - R, \tag{2}$$

which describes a leaky bucket model where ρ_w is the density of liquid water, D is the soil depth, ϕ is non-dimensional soil moisture, P is precipitation, E is evaporation, and R is drainage and runoff. Drainage is parameterized by relaxation toward field capacity (ϕ_{fc}) on a timescale τ_{fc} as

$$R = \max\left[0, \frac{\rho_w D}{\tau_{fc}}(\phi - \phi_{fc})\right]. \tag{3}$$

Runoff is parameterized by immediately resetting soil moisture to the soil porosity (ϕ_{por}) whenever $\phi > \phi_{por}$. We use $\phi_{por} = 0.475$ and $\phi_{fc} = 0.370$, corresponding to values for loamy clay in the Consortium for Small-Scale Modeling (COSMO; Doms et al., 2011), and set $\tau_{fc} = 2$ days. The details of the drainage and runoff parameterizations are unlikely to have important impacts on land-atmosphere coupling because they activate when soil moisture is high and only weakly influences evaporation. Their primary role is simply to allow steady states with $P - E > 0$.

Soil moisture influences evaporation by modulating a surface resistance r_s formulated following Hohenegger and Stevens (2018) as

$$r_s = r_{s,fc}\frac{\phi_{fc} - \phi_{wp}}{\phi - \phi_{wp}}, \tag{4}$$

where $r_{s,fc}$ is the surface resistance at field capacity and ϕ_{wp} is the wilting point soil moisture (Note that an identical model can be obtained by replacing $r_{s,fc}$ and ϕ_{fc} with r_s and ϕ at any reference point.). We use $\phi_{wp} = 0.185$, again

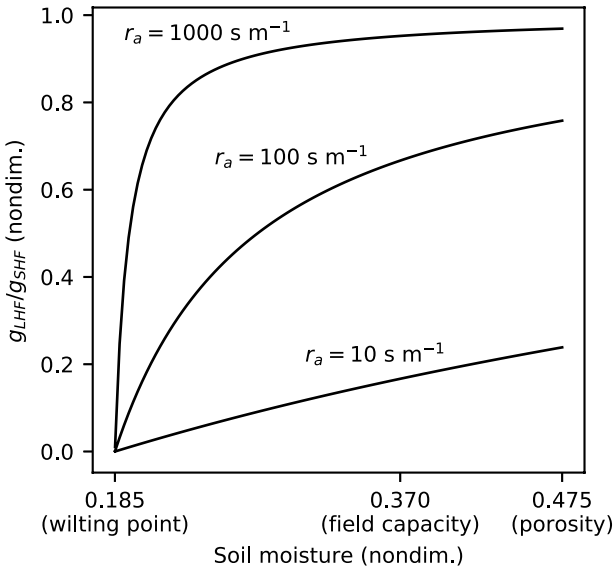

Figure 1. Ratio of the latent to sensible heat flux conductance g_{LHF}/g_{SHF} as a function of soil moisture ϕ for three values of the aerodynamic resistance r_a. Note that $r_a = O(100\ \text{s m}^{-1})$ is typical for the daytime boundary layer in our simulations.

corresponding to the COSMO value for loamy clay, and set $r_{s,fc} = 50\ \text{s m}^{-1}$ so that reductions in soil moisture lead to a gradual shutoff of evaporation (Hohenegger & Stevens, 2018). The surface resistance is added in series to the aerodynamic resistance r_a from Monin–Obhukov similarity theory such that

$$LHF = \rho L_v g_{LHF}(q_s^* - q_a), \tag{5}$$

where ρ is the near surface air density, L_v is the latent heat of vapourization, q_s^* is surface saturation specific humidity, q_a is near-surface specific humidity, and

$$g_{LHF}(\phi) = \frac{1}{r_a + r_s(\phi)} \tag{6}$$

is the latent heat flux conductance. Sensible heat fluxes are given by

$$SHF = \rho c_p g_{SHF}(T_s - T_a), \tag{7}$$

where c_p is the specific heat capacity of dry air, T_s is surface temperature, T_a is near-surface air temperature, and

$$g_{SHF} = \frac{1}{r_a} \tag{8}$$

is the sensible heat flux conductance.

Our choice to use soil texture parameters (ϕ_{por}, ϕ_{fc}, and ϕ_{wp}) corresponding to loamy clay follows Hohenegger and Stevens (2018). These parameters are intermediate choices appropriate for idealized simulations with a single soil type; texture parameters for other soil classes in COSMO vary from $\phi_{por} = 0.364$, $\phi_{fc} = 0.196$, and $\phi_{wp} = 0.042$ (sand) to $\phi_{por} = 0.863$, $\phi_{fc} = 0.763$, and $\phi_{wp} = 0.265$ (peat). Loamy clay is found alongside other soil classes throughout the tropics, including in Central and South America, equatorial Africa, Southeast Asia, and the Maritime Continent (e.g., Ross et al., 2018).

Plotting the ratio of latent to sensible heat flux conductance as a function of soil moisture shows that the latent heat flux conductance (and therefore the latent heat flux itself) goes to zero as soil moisture approaches the wilting point from above (Figure 1). The shutoff occurs more suddenly when the aerodynamic resistance is high (i.e., when the boundary layer is stable, or near-surface wind speeds are low) and more gradually when the aerodynamic resistance is low (i.e., when the boundary layer is unstable, or near surface wind speeds are high). Typical daytime values for the aerodynamic resistance in our simulations are $O(100\ \text{s m}^{-1})$; for these values, the conductance ratio is somewhat sensitive to soil moisture when the surface is wet (i.e., at and above field capacity), but the sensitivity increases substantially below about $\phi = 0.25$. As a result, we expect latent heat fluxes to decrease substantially for $\phi \lesssim 0.25$.

2.2. WTG Parameterization of Large-Scale Dynamics

Our WTG parameterization follows the spectral WTG (SWTG) scheme of Herman and Raymond (2014). At each time step, the scheme diagnoses a large-scale vertical velocity based on differences between horizontally-averaged temperatures and the tropical reference temperature profile, then calculates large-scale tendencies by vertically advecting horizontal-average profiles. While our WTG scheme neglects virtual effects for simplicity, again following the scheme described in Herman and Raymond (2014), virtual effects could be included by calculating the large-scale vertical velocity profile based on virtual temperature anomalies. The net effect of the parameterized large-scale circulation produced by our WTG scheme is to relax domain-mean temperatures toward a reference tropical-mean temperature profile while generating internally self-consistent profiles of large-scale moisture convergence and divergence that produce an open hydrological cycle. This parameterization is critical for our work because it allows simulations to support both precipitating equilibria with active deep convection and non-precipitating equilibria where convection is inactive throughout the entire model domain.

The large-scale vertical velocity is set by diagnosing the displacement D_{WTG} required to nullify the domain-mean dry static energy perturbation of the atmospheric layer at height z. This is given by

$$D_{WTG}(z) = \frac{\bar{s} - s_0}{\max(c_p\gamma, \partial_z \bar{s})}, \tag{9}$$

where $\bar{s}$ is the horizontally-averaged dry static energy (DSE), s_0 is a reference DSE profile calculated from the reference tropical-mean temperature profile, z is height, c_p is the heat capacity of dry air, and $\gamma = 0.3$ K km^{-1} is a minimum stability intended to prevent unrealistically-large vertical velocities at levels with weak stability. D_{WTG} is then projected onto a series of approximate gravity wave modes, giving

$$\hat{D}_{WTG,j} = \frac{2}{H}\int_0^H D_{WTG}(z)\sin\left(\frac{j\pi z}{H}\right)\mathrm{d}z, \tag{10}$$

and the large-scale vertical velocity w_{WTG} is reconstructed from $\hat{D}_{WTG}$ as

$$w_{WTG}(z) = \sum_j \frac{\hat{D}_{WTG,j}}{\tau_j}\sin\left(\frac{j\pi z}{H}\right). \tag{11}$$

The tropopause height H is set to the height of the lower interface of the model level at which domain-average temperatures first drop below 210 K, and we include modes from $j = 1$ to the number of model levels below $z = H$. With this set of modes, the smallest height scales in w_{WTG} are equal to the average vertical resolution of the model between the surface and $z = H$ (about 400 m for typical values of H). We set w_{WTG} to zero above $z = H$. The relaxation timescale τ_j is mode-dependent and set to

$$\tau_j = \frac{L}{c_j} \tag{12}$$

where L is a specified horizontal length scale. c_j is the hydrostatic gravity wave speed corresponding to mode j, estimated as

$$c_j = \frac{NH}{\pi j}, \tag{13}$$

where N is the average of the Brunt-Vaisala frequency between $z = 0$ and $z = H$. We set $L = 128$ km, equal to the horizontal extent of the model domain. Once w_{WTG} is known, large-scale tendencies for a generic scalar ϕ are calculated as

$$\dot{\phi}(x, y, z) = -w_{WTG}(z)\frac{\partial\bar{\phi}(z)}{\partial z}, \tag{14}$$

where $\bar{\phi}$ indicates a horizontal average over the model domain. We include large-scale tendencies for all water species and liquid/ice static energy, the prognostic thermodynamic variable used by SAM.

A primary goal of this paper is to examine whether simulated soil moisture-precipitation feedbacks are robust to details in the formulation of WTG parameterizations of large-scale dynamics—much as a study using a global climate model might examine robustness to details in the formulation of sub-grid parameterizations—and formulating the SWTG scheme described in this section required making some decisions about details. Here, we provide the reasoning behind key decisions, and we examine the impact of some of these decisions in more detail in Section 5.

Rather than using an SWTG scheme, we could have chosen to use a simpler conventional WTG (CWTG) scheme (Herman & Raymond, 2014; Raymond & Zeng, 2005) that simply sets $w_{WTG} = D_{WTG}/\tau_1$. We focus initially on SWTG simulations for two reasons. The first is that CWTG schemes require manually tapering w_{WTG} so that it satisfies $w_{WTG} = 0$ at $z = 0$ and $z = H$, and past work indicates that the presence of multiple equilibria in CWTG simulations over fixed sea surface temperatures can be sensitive to how this tapering is accomplished (Daleu et al., 2015; Herman & Raymond, 2014). The second is that SWTG schemes produce a nonlocal response to temperature anomalies, an effect present in fully-resolved large-scale circulations that can alter how large-scale flow interacts with convection and cannot be captured by CWTG schemes (Herman & Raymond, 2014; Romps, 2012a). We could also have chosen to use a weak pressure gradient (WPG, Edman & Romps, 2014; Kuang, 2008; Romps, 2012a) scheme in place of a WTG scheme. WPG schemes are similar to SWTG schemes

in that they capture the nonlocal response to transient buoyancy anomalies, but are derived by parameterizing the pressure gradient force between the model domain and surrounding environment and damp shallow buoyancy anomalies less quickly than either SWTG or CWTG schemes (Herman & Raymond, 2014; Romps, 2012b). We focus on simulations with WTG schemes primarily because this provides a stronger connection with past studies that motivate our work (Anber, Gentine, et al., 2015; Sessions et al., 2010; Sobel et al., 2007), but we include some discussion of how using a WPG scheme might affect model behavior in the concluding section of our paper (Section 6).

We also could have chosen to calculate large-scale tendencies to include convergence from a reference column with properties that differ from averages over the model domain (Romps, 2012a; Sessions et al., 2010, 2015, 2016). We chose our formulation of large-scale tendencies primarily because it requires minimal additional information—in particular, it does not require determining an appropriate moisture profile for surrounding regions—and so is simpler to implement in less idealized experiments (e.g., Anber, Gentine, et al., 2015) where reference profiles are taken from observations. Additionally, this choice introduces an important distinction between our simulations and RCE simulations with resolved soil moisture gradients, because it prevents dry states in our simulations from re-moistening by converging moisture from a surrounding wetter region. One potential downside of our formulation is that it provides no way for the atmosphere to remoisten from a state where the atmosphere is completely dry and evaporation from the surface is completely shut off. To ensure our simulations never access this state, we add an additional large-scale tendency given by

$$\dot{q}_{v,relax}(x, y, z) = \max[0, \beta(q_0(z) - \bar{q}_v(z))] \tag{15}$$

to the specific humidity field to prevent complete drying of the atmosphere. $q_0(z)$ is set to correspond to 10% relative humidity for the tropical reference temperature profile, and β is set to (5 days)$^{-1}$ below $z = H - 2$ km and tapered linearly to zero at $z = H$.

2.3. Model Constraints in Equilibrium

To summarize: the combination of an interactive land-like surface and WTG parameterization of large-scale flows allow our simulations to attain both precipitating and non-precipitating steady states, but requires them to do so in a way that satisfies energy and moisture balances for both the surface and the atmosphere:

1. *Surface energy balance*. In equilibrium, surface heating by shortwave and downwelling longwave radiation must be balanced by surface cooling by longwave emission and turbulent fluxes, which constrains the equilibrium surface temperature.
2. *Surface moisture balance*. When soil moisture is prognostic, surface moistening by precipitation must be balanced at equilibrium by moisture loss through evaporation, drainage, and runoff. This permits precipitating steady states with precipitation either equal to or greater than evaporation. In the former case ($P - E = 0$), soil moisture can in principle assume any value between the wilting point and field capacity. In the latter case, positive $P - E$ must be balanced by drainage and runoff, which requires soil moisture to be at or above field capacity. In non-precipitating steady states ($P = 0$), the only possible equilibrium is one with $E = 0$, so soil moisture must decrease until it reaches the wilting point and evaporation shuts off.
3. *Atmospheric energy balance*. In precipitating steady states with active deep convection, convective heating can exceed radiative cooling (in which case the residual is balanced by cooling by large-scale ascent) or be somewhat smaller than radiative cooling (in which case the residual is balanced by heating by large-scale subsidence). In non-precipitating steady states, a steady-state atmospheric energy budget is achieved through a balance between radiative cooling and heating by large-scale subsidence.
4. *Atmospheric moisture balance*. In precipitating steady states, non-zero $P - E$ can be balanced by large-scale moisture convergence or divergence. In non-precipitating steady states, non-zero E (permissible at equilibrium only when soil moisture is fixed) must be balanced by large-scale moisture divergence. This is accomplished through large-scale subsidence (required for atmospheric energy balance) that produces low-level mass divergence in a moist boundary layer.

3. Multiple Equilibria With Fixed Soil Moisture

We begin by running a suite of simulations with interactive surface temperature and soil moisture fixed at field capacity. Insolation is set to an equinoctial diurnal cycle, and we vary the solar latitude to obtain simulations

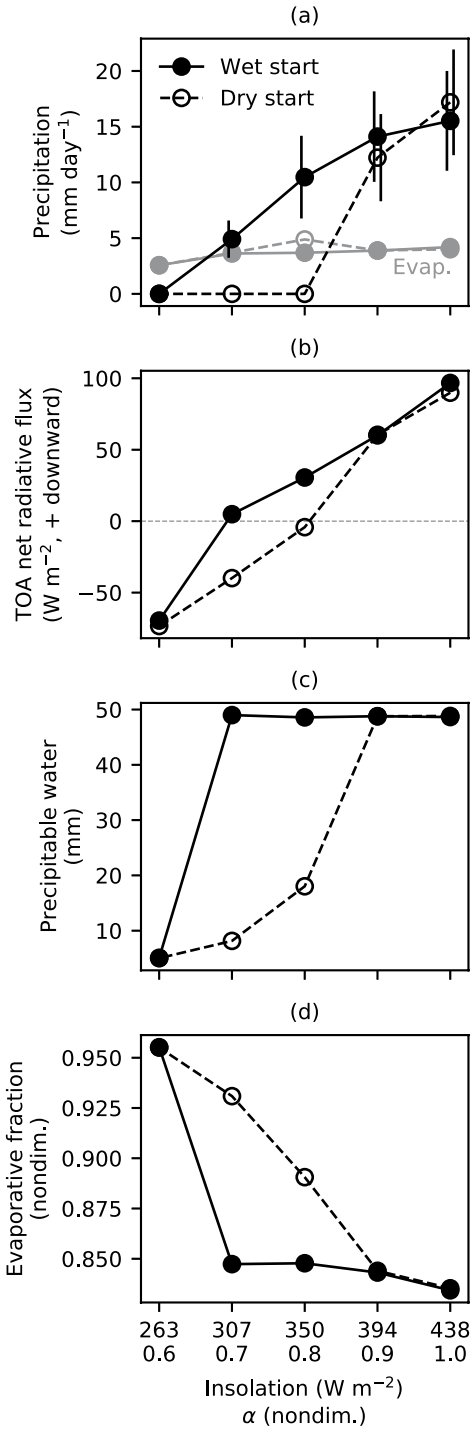

Figure 2. Domain- and time-average precipitation and evaporation (a), top-of-atmosphere net radiative flux (b), precipitable water (c), and surface evaporative fraction (d) from the last 20 days of simulations initialized with a humid atmosphere (solid lines) and with a dry atmosphere (dashed lines). Vertical black lines in panel (a) show ±1 standard error of daily-average precipitation rates.

with time-mean insolation $I = \alpha I_0$ for $\alpha = (1, 0.9, 0.8, 0.7, 0.6)$, where $I_0 = 438.6$ W m^{-2} is the time-mean insolation at a solar latitude of 0°. At each solar latitude, we test for the presence of multiple equilibria by comparing simulations initialized with the mean moisture profile from the last 20 days of the RCE simulation to simulations initialized with a completely dry atmosphere.

Equilibration time scales in our WTG simulations are quite short. Most reach a statistically-steady state within the first 20 days of simulation, much faster than the time required for the equilibration of RCE simulations over interactive surfaces (Cronin & Emanuel, 2013; Romps, 2020). To ensure that equilibria are robust over longer time scales, however, we allow simulations to run for 80 days before collecting statistics over days 80–100. With a humid initial atmosphere, simulations reach a precipitating equilibrium for $\alpha \geq 0.7$; with a dry initial atmosphere, simulations remain dry for $\alpha \leq 0.8$ (Figure 2a). Thus, similar to findings over fixed-temperature ocean surfaces (Sessions et al., 2010; Sobel et al., 2007), WTG simulations over a moist land surface can support multiple equilibria in precipitation, and the relatively short equilibration time scales suggest that they might manifest during relatively short periods of undisturbed conditions. For brevity, we will refer to these as "wet" and "dry" equilibria even though the surface evaporates freely in all cases.

Precipitation minus evaporation is positive in all wet equilibria, indicating large-scale moisture convergence, and negative in all dry equilibria, indicating large-scale moisture divergence (Figure 2a). The top-of-atmosphere net radiative flux (equivalent to the net radiative energy input into the column) is positive in wet equilibria and negative in dry equilibria (Figure 2b), giving a positive normalized gross moist stability (Raymond et al., 2009) in all equilibrium states. Precipitable water is much lower in dry equilibria than in wet equilibria due to free-tropospheric drying by large-scale subsidence (Figure 2c). The surface evaporative fraction ($LHF/(LHF + SHF)$) is relatively high in both wet and dry equilibria because soil moisture is fixed at field capacity (Figure 2d).

In wet equilibria, the time-mean dry static energy anomaly and WTG vertical velocity are positive in the upper troposphere but negative in the lower troposphere (Figures 3a and 3c), with lower-tropospheric subsidence likely linked to evaporative cooling by precipitation (Romps, 2012a). Stronger large-scale ascent in the upper troposphere coincides with increases in cloud fraction and relative humidity (Figures 3e and 3g). Radiative cooling decreases below extensive upper-tropospheric cloud layers and increases above them (Figure 3i). In dry equilibria, the time-mean dry static energy anomaly is small in the free troposphere and mostly negative in the boundary layer, except near the surface at relatively high insolation (Figure 3b). Large-scale subsidence is weak in the free troposphere and somewhat stronger near the surface, except at relatively high insolation where a shallow ascending layer forms (Figure 3d). The atmosphere is cloud-free, relative humidity is low in the free troposphere but somewhat higher in the boundary layer, and radiative cooling is around 1 K day^{-1} in the free troposphere with a peak near the top of the boundary layer (Figures 3f, 3h, and 3j).

Time-mean surface temperatures are higher in wet equilibria than in dry equilibria, but more sensitive to increases in insolation in dry equilibria than in wet equilibria (Figure 4a). Both features can be understood at least empirically in terms of surface heating by radiative fluxes (net shortwave plus downward longwave fluxes at the surface, Figure 4b) and MSE in the near-surface atmosphere (Figure 4c). Higher surface radiative heating requires a larger

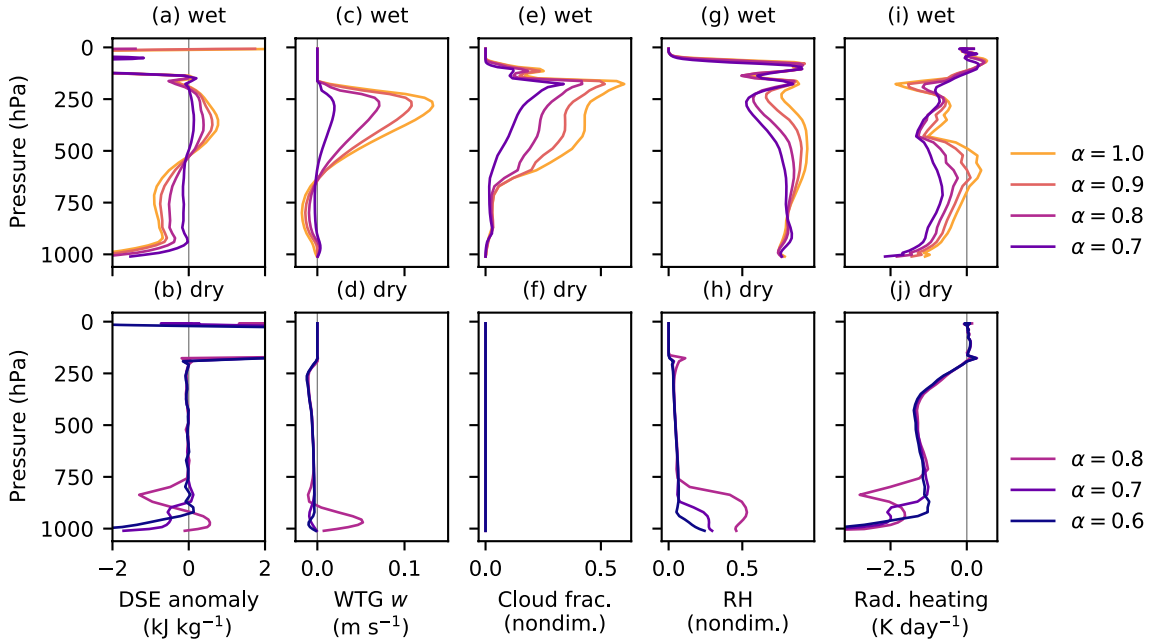

Figure 3. Time- and domain-mean dry static energy anomaly (a, b), weak temperature gradient vertical velocity (c, d), cloud fraction (e, f), relative humidity (g, h), and radiative heating (i, j) in wet equilibria (top) and dry equilibria (bottom). All profiles are averages over the last 20 days of simulation.

surface-atmosphere disequilibrium to maintain surface energy balance, and higher near-surface MSE requires higher surface temperatures to maintain a given surface-atmosphere disequilibrium. In dry equilibria with low insolation, surface radiative heating is relatively low because of limited downward longwave emission from the dry free troposphere, and near-surface MSE is relatively low because of boundary layer drying by large-scale subsidence. However, both surface radiative heating and near-surface MSE increase quickly with increasing insolation as surface heating increases and the boundary layer becomes deeper and moister. As a result, surface temperatures in dry equilibria are low at low insolation but increase rapidly with increasing insolation. In wet equilibria with low insolation, surface radiative heating is relatively high because the free troposphere is relatively moist, and convection maintains relatively high near-surface MSE in a convectively-coupled boundary layer. As insolation increases, increasing cloud cover limits increases in surface radiative heating, and near-surface MSE drops, likely due to increased cooling by precipitation-driven downdrafts. As a result, surface temperatures in wet equilibria are relatively high at low insolation but actually decrease slightly as insolation increases.

Finally, we note that while convection in wet equilibria remains disaggregated, boundary layer humidity in dry equilibria organizes into distinct moist and dry regions at low insolation (Figure 5). Analysis of the moisture budget for (16 km)^2 mesoscale blocks, following Bretherton and Blossey (2017), suggests that organization is associated with upgradient moisture transport by boundary layer circulations: vertical advection of the domain-averaged moisture profile increases the precipitable water anomaly in the moistest quartile of mesoscale blocks by more than 0.3 mm day^{-1} in the simulations where organization occurs, and by just 0.1 mm day^{-1} in the simulation where organization does not occur (not shown). We have not analyzed the boundary layer circulations in detail, but a plausible driver is reduced radiative cooling in relatively moist regions of the boundary layer (Naumann et al., 2019).

4. Negative Soil Moisture-Precipitation Feedbacks From Surface Drying

The surface moisture budget is out of balance in both the wet and dry equilibria documented in the previous section. In wet equilibria, precipitation exceeds evaporation, and the surface acts as a moisture sink. Because the evaporative fraction is already high, however, allowing soil moisture to evolve in time does not significantly modify the wet state: soil moisture simply increases until drainage and runoff balance precipitation minus evaporation, and evaporation remains high (not shown). In dry equilibria, in contrast, evaporation exceeds precipitation, and the surface acts as a moisture source. In this case, allowing soil moisture to evolve in time will significantly

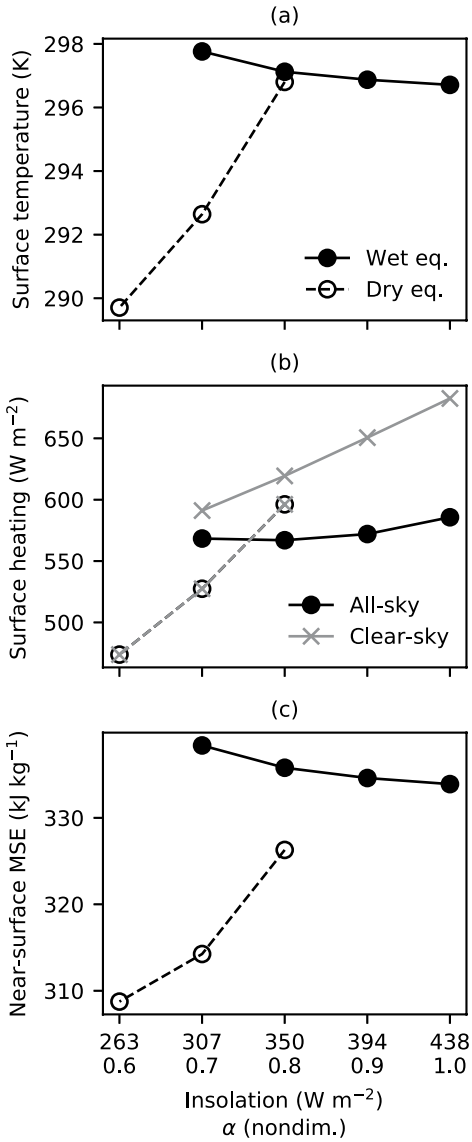

Figure 4. Domain- and time-average surface temperature (a), surface radiative heating (b), and near-surface moist static energy (c) from the last 20 days of simulations that attain wet equilibria (solid lines) and dry equilibria (dashed lines). In panel (b), black lines show surface heating by all-sky radiative fluxes and gray lines show surface heating by clear-sky radiative fluxes.

alter the dry state: as the surface dries, latent heat fluxes will gradually be replaced by sensible heat fluxes. In this section, we test whether dry equilibria persist as the surface dries out, or whether surface drying can trigger a transition back to a precipitating state.

Specifically, we continue by restarting simulations from dry equilibria, but with interactive soil moisture. We set the soil depth D to 1 m. This value is chosen to be large enough to avoid substantial changes in evaporative fraction over a single diurnal cycle, but small enough to allow soil moisture to equilibrate over a timescale of several tens of days. Other boundary conditions are left unchanged when simulations are restarted. For $\alpha = 0.7$ and 0.8 (where both wet and dry equilibria exist with fixed soil moisture), we find that a transient reduction in evaporative fraction (associated with surface drying) triggers a transition back to an unaggregated precipitating equilibrium (Figure 6). Lower insolation requires lower evaporative fraction before the transition occurs. This transition is a form of a negative soil moisture-precipitation feedback: surface drying triggers the onset of precipitation, which remoistens the surface. For $\alpha = 0.6$ (which does not support a wet equilibrium with fixed soil moisture) the simulation remains non-precipitating, including if the simulation is extended for an additional 100 days.

To assess whether transitions from non-precipitating to precipitating states are sensitive to the initial conditions used to restart simulations, we run additional simulations with $\alpha = 0.7$ and $\alpha = 0.8$, but restarted from the dry equilibrium state obtained with fixed soil moisture at $\alpha = 0.6$ (For brevity, we refer to these simulations as "controlled initial condition" experiments moving forward.). We find that controlling for differences in initial conditions has little effect on the long-term evolution of the simulations. Evaporative fractions appear to lose memory of initial conditions after a ~5–10 day adjustment period, and the timing of transitions to precipitating equilibria is insensitive to differences in initial conditions (Figure 6).

To illustrate how the dry state changes as the surface dries out, we define boundary layer specific humidity (q_b), boundary layer DSE (s_b), and boundary layer MSE (h_b) as mass-weighted averages over every grid point in the lowest kilometer of the atmosphere, and we plot trajectories in a phase space using q_b and s_b as axes. We include points at 18 local solar time (LST) on each day, when h_b is close to its diurnal maximum, and end trajectories after 100 days or when the daily-average precipitation rate exceeds 1 mm day^{-1} anywhere in the model domain. These trajectories suggest that the transition back to a precipitating equilibrium is linked to changes in thermodynamic properties of the boundary layer: as the surface dries, both s_b and q_b increase, producing an increase in h_b that eventually permits the onset of deep convection (Figure 7a). For a given α, transitions to precipitating equilibria (endpoints labeled "wet" in Figure 7) occur at nearly identical locations in phase space regardless of the initial condition, and are preceded by nearly-identical trajectories (compare solid and dashed lines in Figure 7a).

The increase in s_b is an unsurprising consequence of surface drying, which increases surface temperature and sensible heat fluxes. The increase in q_b is more surprising, because it occurs despite a reduction in evaporation, and we devote the rest of this section to examining why q_b increases as the surface dries out. The point we will pursue is that q_b is influenced both by evaporation (which moistens the column) and by large-scale subsidence (which dries the column), and that a decrease in evaporation need not necessarily lead to a drier atmosphere if drying by large-scale subsidence simultaneously becomes weaker.

To begin, we note that the domain-average precipitable water budget in non-precipitating states (neglecting relatively small contributions of at most 0.4 mm day^{-1} from humidity relaxation in the free troposphere) is

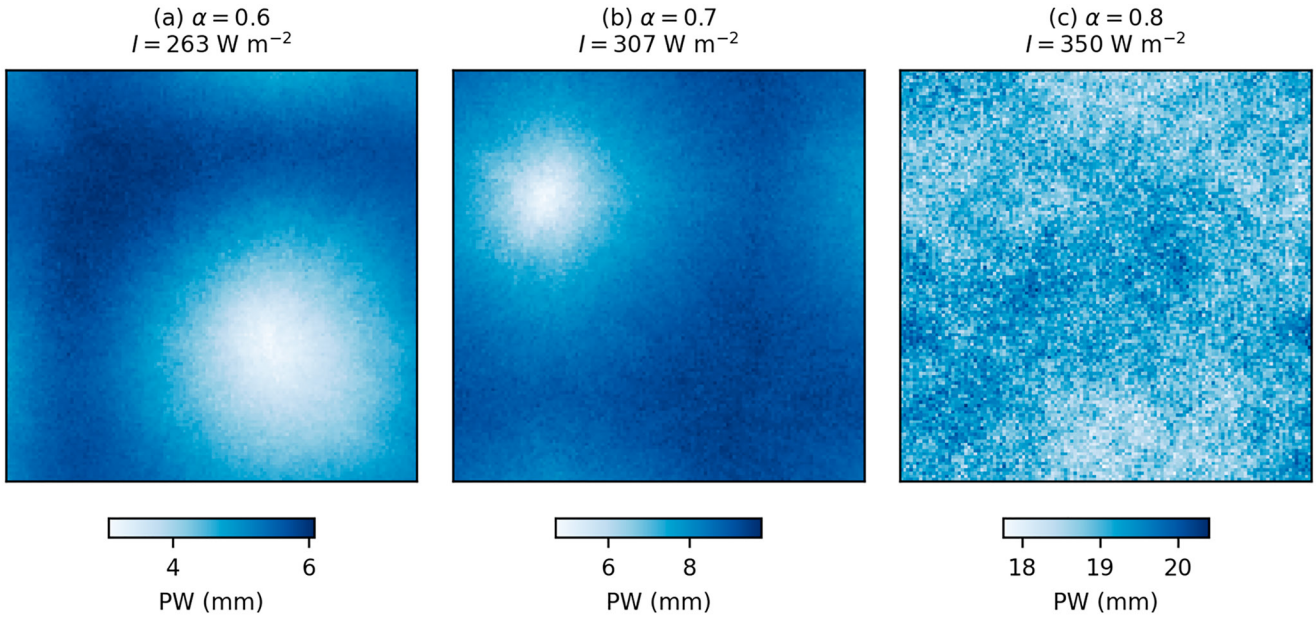

Figure 5. One-hour-average precipitable water (plan view) at midnight on the last day of each simulation of dry equilibria.

$$\frac{\mathrm{d}PW}{\mathrm{d}t} = E - \int_0^H \rho w_{WTG} \frac{\partial \bar{q}_v}{\partial z} \mathrm{d}z, \tag{16}$$

where PW is precipitable water, E is evaporation, and ρ is density. This equation links changes in evaporation and subsidence drying to changes in precipitable water, but not directly to q_b. To develop a connection with q_b, we re-write the budget as

$$\frac{\mathrm{d}PW}{\mathrm{d}t} = E - M_{vent} \overline{q_{vs}}, \tag{17}$$

where $\bar{q_{vs}}$ is domain-average specific humidity at the surface, and the ventilation mass flux M_{vent} is given by the moisture-gradient-weighted average of the WTG mass flux as

$$M_{vent} = \left(\int_0^H \rho w_{WTG} \frac{\partial \bar{q}_v}{\partial z} \mathrm{d}z \right) / \left(\int_0^H \frac{\partial \bar{q}_v}{\partial z} \mathrm{d}z \right) = \frac{1}{\overline{q_{vs}}} \int_0^H \rho w_{WTG} \frac{\partial \bar{q}_v}{\partial z} \mathrm{d}z. \tag{18}$$

This equation assumes that $\overline{q_v} \approx 0$ at $z = H$. If the boundary layer is well-mixed, we expect that $\overline{q_{vs}} \approx q_b$, giving

$$\frac{\mathrm{d}PW}{\mathrm{d}t} \approx E - M_{vent} q_b. \tag{19}$$

This equation captures the following idea: for a given E (set by surface energy balance and soil moisture) and M_{vent} (set primarily by the large-scale mass flux at the top of the boundary layer, where the vertical humidity gradient is large), achieving a steady-state precipitable water budget requires increasing boundary layer moisture (q_b) until the moisture gradient at the top of the boundary layer is large enough for subsidence drying to balance moistening by evaporation. This interpretation suggests that a useful phase space for visualizing the combined effects of changes in evaporation and subsidence drying is one with E and M_{vent} as axes. In this space, an increase in the ratio E/M_{vent} indicates that evaporation and the subsidence mass flux are co-evolving in a way that requires an increase in q_b to return to a steady state. Our simulations are not in steady state as the surface dries, so we do not expect E/M_{vent} to track the diagnosed value of q_b exactly, but we do expect simulations to evolve toward a state with higher q_b if E/M_{vent} increases over time.

Trajectories in E-M_{vent} space show that the ratio E/M_{vent} can increase by a factor of two or more as the surface dries (Figure 7b), qualitatively consistent with diagnosed increases in boundary layer q_b. As expected, the time

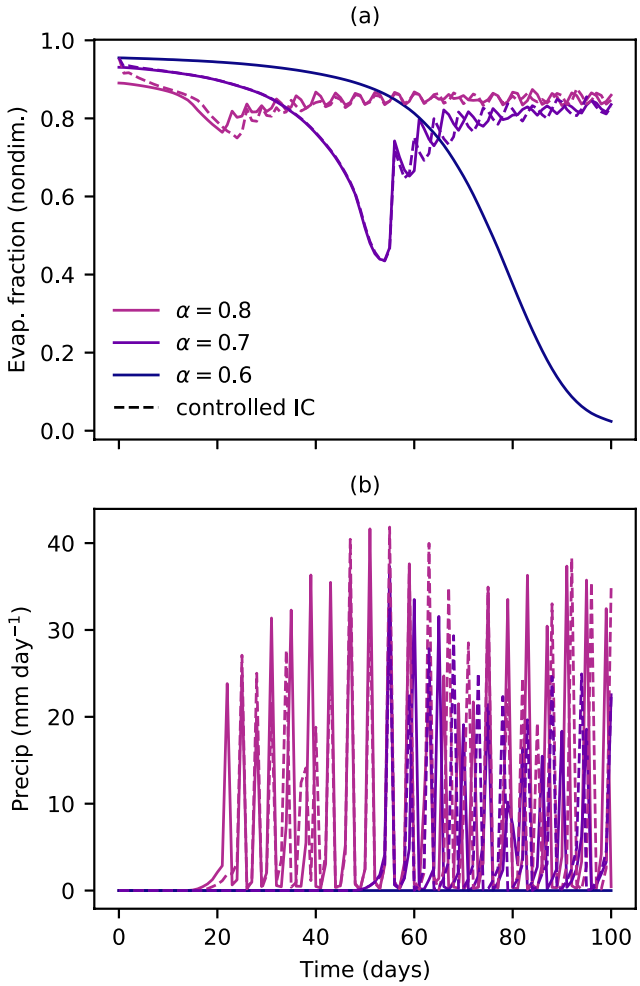

Figure 6. Time series of 24-hr-average evaporative fraction (a) and precipitation (b) in simulations restarted from dry equilibria with interactive soil moisture. Solid lines show time series from restart experiments with different initial conditions for different values of α, and dashed lines show time series from controlled initial condition experiments restarted from dry equilibria obtained with fixed soil moisture and $\alpha = 0.6$.

evolution of E/M_{vent} is not a precise quantitative match to the time evolution of q_b. Variations in q_b lag variations in E/M_{vent}, and E/M_{vent} tends to slightly overestimate q_b even when the time rate of change of q_b is small because the boundary layer is not always well-mixed near the surface (Figure 8). However, the evolution of E/M_{vent} captures key qualitative features of the evolution of q_b, including increases preceding the onset of precipitation at $\alpha = 0.7$ and 0.8, and a transient increase followed by a decrease at $\alpha = 0.6$. In both cases, increases in boundary layer humidity are driven by decreases in M_{vent} that occur as the surface dries but before evaporation completely shuts off.

To further investigate why the ventilation mass flux decreases as the surface dries out, we plot single-day time series of M_{vent} over the last day of the $\alpha = 0.6$ simulation used to generate the initial condition used for controlled-initial-condition restart experiments (larger circles in Figure 7), and on later days during controlled-initial-condition restart experiments (crosses in Figure 7) when E/M_{vent} has become substantially larger. During the last day of the experiment used to generate the initial condition, the ventilation mass flux is positive (indicating boundary layer drying by the large-scale flow) throughout the day. As the surface dries during restart experiments, however, the ventilation mass flux switches sign from positive to negative (indicating boundary layer moistening by the large scale flow) during the 6 hr following solar noon (Figure 9).

Examining boundary layer profiles at 15 LST (3 hr since solar noon) on the days plotted in Figure 9 suggests that negative ventilation mass fluxes during the afternoon are associated with positive near-surface DSE anomalies produced by an increase in boundary layer temperature as the surface dries (Figures 10a–10c). Near the top of the boundary layer, DSE anomalies are negative and the magnitude of D_{WTG} (i.e., the vertical distance that air must be displaced to nullify the DSE anomaly) is relatively small because stability is relatively high (Figures 10d–10f). The magnitude of D_{WTG} is much larger near the surface, where it is set by the DSE anomaly and the minimum stability parameter γ, which limits the strength of vertical motion within the nearly-neutrally-stable boundary layer. (Note that the DSE *anomaly* does not have to be vertically uniform for stability to be low because the WTG reference profile contains only a shallow boundary layer.) The non-local response to near-surface increases in D_{WTG} produces strong ascent within the boundary layer and weak ascent—but ascent nonetheless—at the boundary layer top (Figures 10g–10i), where the vertical specific humidity gradient is largest (Figures 10j–10l). Ascent in well-mixed portions of the boundary layer, although possibly unphysically strong, produces relatively small large-scale tendencies because large-scale vertical motion interacts with the rest of the model only through the vertical advection of energy and moisture. In contrast, much weaker ascent at the boundary layer top and below about 950 hPa (where the boundary layer is not well mixed) produces substantial moisture sources. The net result is moisture import, rather than export, by the large-scale flow (Figures 10m–10o).

To summarize: before soil moisture decreases, dry equilibria are maintained by large-scale subsidence that ventilates the boundary layer and prevents evaporation from re-moistening the atmosphere. Decreasing soil moisture leads to decreasing evaporation, which by itself would lead to further drying of the boundary layer. However, lower soil moisture also leads to warming of the surface and boundary layer, which weakens parameterized subsidence and eventually produces low-level ascent during the afternoon. These changes reduce boundary layer ventilation (drying) by the large-scale circulation and lead to boundary layer moistening, despite reduced surface evaporation. The combination of boundary layer moistening and warming leads to increases in boundary layer MSE, which increases convective instability and eventually leads to the onset of convection and precipitation. There are limitations to this analysis. It is diagnostic, not predictive, and does not (e.g.,) explain why weaker boundary layer drying by large-scale subsidence more than compensates for weaker moistening by evaporation. It

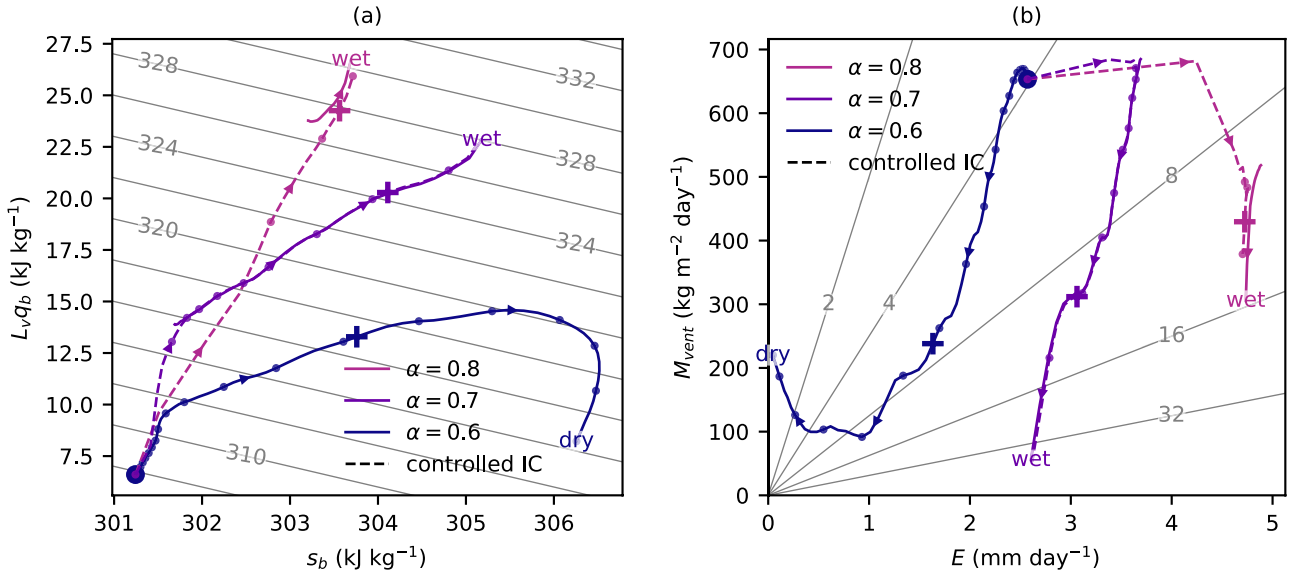

Figure 7. Trajectories of simulations restarted from dry equilibria with interactive soil moisture in phase spaces using boundary layer DSE and moisture (a) and evaporation and ventilation mass flux (b) as axes. Solid lines show trajectories from restart experiments with different initial conditions for different values of α, and dashed lines show time series from controlled initial condition experiments. Gray lines in panel (a) are contours of constant boundary layer moist static energy (units of kJ kg^{-1}, increasing by increments of 2 kJ kg^{-1} moving upwards), and gray lines in panel (b) are contours of constant E/M_{vent} (units of g kg^{-1}, increasing by factors of 2 moving clockwise). Trajectories evolve in the directions indicated by arrows. Endpoints labeled "dry" denote trajectories that end after 100 days in a dry state, and endpoints labeled "wet" denote trajectories that end because of the onset of precipitation (details in text). Trajectories in panel (a) include points taken at 18 local solar time on each day, and trajectories in panel (b) include 24 hr averages for each day. Large circles and crosses show, respectively, the controlled initial condition and points along trajectories examined in more detail in subsequent figures. Small circles show 5 day increments along trajectories started from the controlled initial condition.

also relies on a domain-mean perspective that ignores boundary layer organization in dry states (recall Figure 5). Nevertheless, it provides a basic understanding of a surprising result: that surface drying can trigger a transition from a non-precipitating state back to a precipitating state.

5. Sensitivity to the Large-Scale Dynamics Parameterization

In the previous section, we showed that surface drying can trigger a transition from a dry state to a precipitating state in simulations with parameterized large-scale dynamics. Our analysis suggests that the transition is enabled

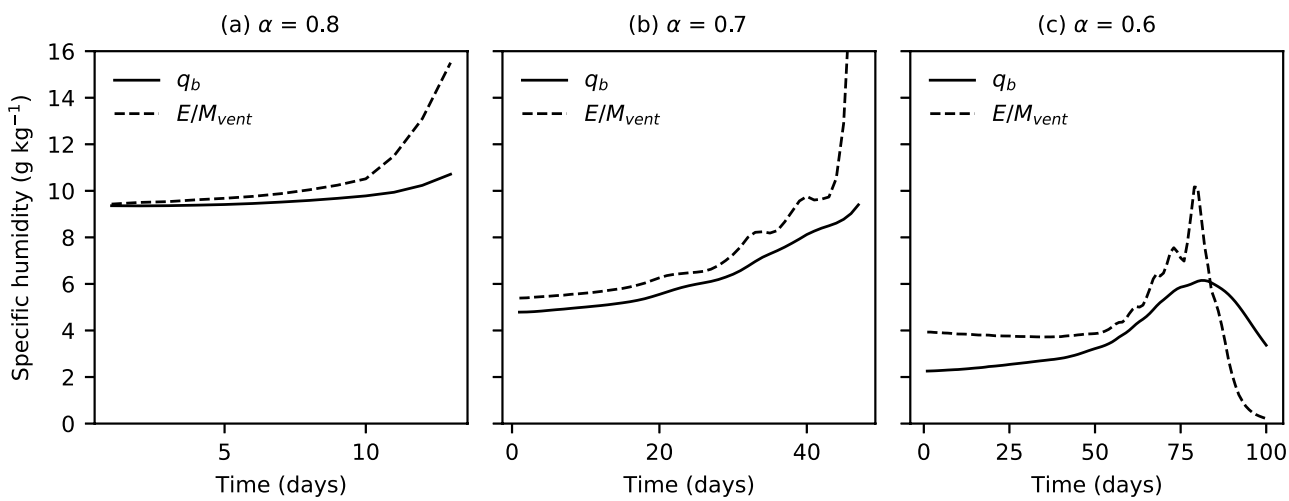

Figure 8. Time evolution of q_b (solid) and E/M_{vent} (dashed) in restart experiments with different initial conditions for different α. Time series are terminated when precipitation exceeds 1 mm day^{-1} anywhere in the model domain (panels a and b) or after 100 days (panel c).

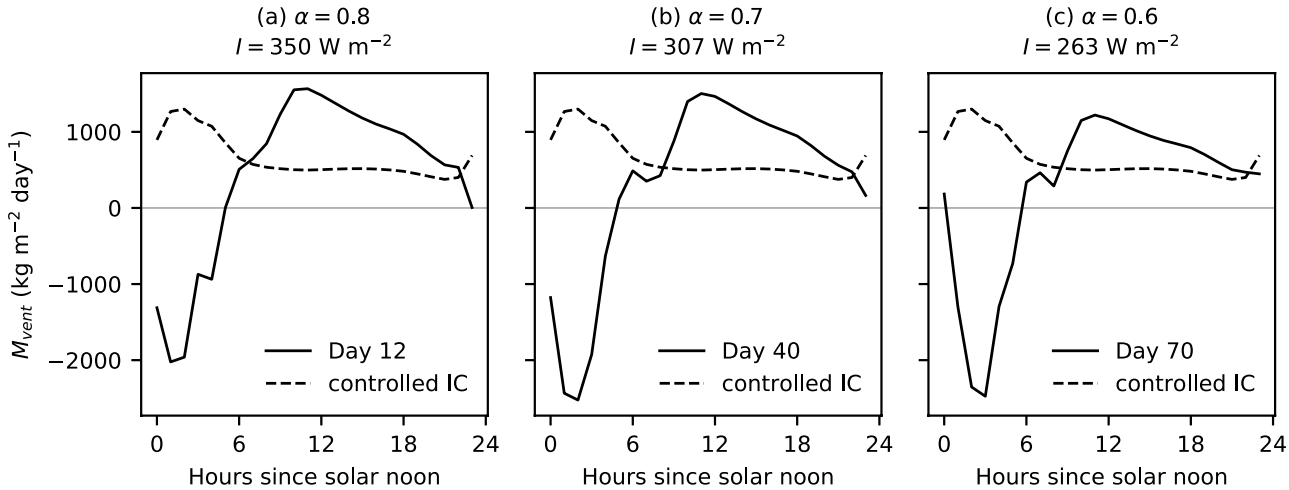

Figure 9. Single-day time series of the ventilation mass flux on the last day of the $\alpha = 0.6$ simulation used to generate the initial condition for controlled-initial-condition restart experiments (dashed lines, marked by large circles in Figure 7) and later days during controlled-initial-condition restart experiments (solid lines, marked by crosses in Figure 7).

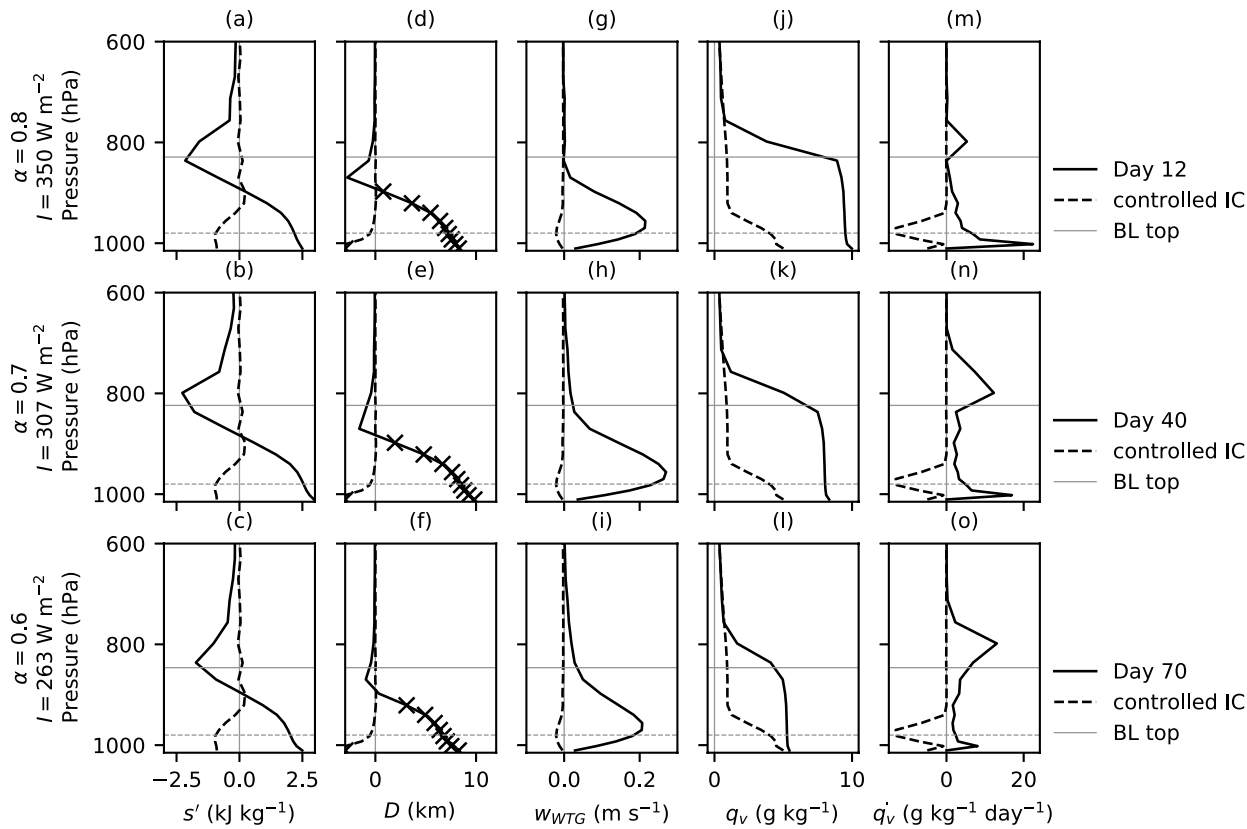

Figure 10. Boundary layer profiles at 15 local solar time on the last day of the simulation used to generate the initial condition for controlled-initial-condition restart experiments (dashed lines, marked by large circles in Figure 7) and on later days during controlled-initial-condition restart experiments (marked by crosses in Figure 7). Panels (a–c) show the dry static energy anomalies relative to the weak temperature gradient (WTG) reference profile, panels (d–f) show D_{WTG} diagnosed from the dry static energy anomaly, panels (g–i) show the WTG vertical velocity calculated from D_{WTG}, panels (j–l) show domain-average specific humidity, and panels (m–o) show the WTG moisture tendency calculated from the WTG vertical velocity and domain-average specific humidity. X's in the second column mark regions where D_{WTG} is limited by the minimum stability parameter γ. Thin gray lines show the boundary layer top for the initial condition (dashed) and on later days (solid), defined as the lowest level with domain-average specific humidity below 80% of its value in the lowest model level.

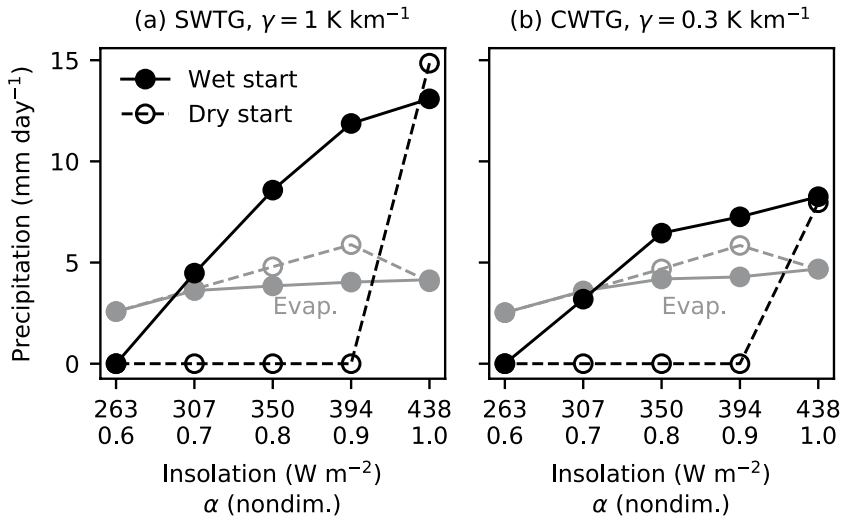

Figure 11. As in Figure 2a, but for simulations using the alternative spectral WTG (SWTG) scheme (a) and the conventional WTG (CWTG) scheme (b).

by interactions between surface drying, near-surface DSE anomalies, and large-scale vertical motion near the top of the boundary layer. However, we want to emphasize that there are reasons to be cautious about the robustness of the response to surface drying. Some skepticism is warranted particularly because the transition from a dry to a precipitating state is influenced by changes to the near-surface large-scale circulation, where the basic assumptions underlying the WTG parameterization (i.e., that fast gravity wave speeds lead to small horizontal temperature gradients) are least valid, and where the parameterization requires some fixes (notably the specification of a minimum stability) to produce finite vertical velocities.

In particular, our analysis of the transition from a dry state to a precipitating state suggests that the transition might be less likely to occur with a WTG parameterization that uses a larger value for the minimum stability parameter, or that only allows a local response of the vertical velocity to DSE anomalies. Increasing the minimum stability parameter should result in a smaller D_{WTG} for a given DSE anomaly in a neutrally-stable boundary layer, and so might reduce the strength of large-scale ascent near the surface and the top of the boundary layer. Allowing only a local response to DSE anomalies would link large-scale ascent at the top of the boundary layer to DSE at the top of the boundary layer, and so might prevent near-surface DSE anomalies from inducing ascent at the top of the boundary layer where vertical moisture gradients are strongest. To be clear: the non-local relationship between DSE anomalies and large-scale ascent is a feature of SWTG schemes (Herman & Raymond, 2014), not a bug, but exploring robustness to the presence of this feature is still worthwhile.

We test the effect of these two changes by repeating our experiments with two alternative WTG schemes. One alternative scheme is an SWTG scheme, unchanged except that γ is increased from 0.3 to 1 K km^{-1}. The other alternative scheme is a CWTG scheme, again following Herman and Raymond (2014). The structure of and parameters in the CWTG scheme are identical to the SWTG used in previous sections, except that w_{WTG} is calculated as

$$w_{WTG}(z) = \sin\left(\frac{\pi z}{H}\right)\frac{D_{WTG}(z)}{\tau_1} \tag{20}$$

for 1 km $< z < H$, set to 0 for $z > H$, and tapered linearly to zero at the surface from its value at 1 km.

Simulations using the alternative SWTG scheme and CWTG scheme share some qualitative features with simulations using the original SWTG scheme. Multiple equilibria experiments with soil moisture fixed at field capacity still produce bistability at intermediate insolation (Figure 11), and surface drying in simulations restarted from dry equilibria with interactive soil moisture still, in some cases, results in a transition back to a precipitating state (Figure 12). However, both the alternative SWTG scheme and the CWTG scheme differ from the original SWTG scheme in that they support dry equilibria with fixed soil moisture at relatively-higher insolation, and in that some bistability remains even when soil moisture is made interactive. The evolution of boundary layer properties as the

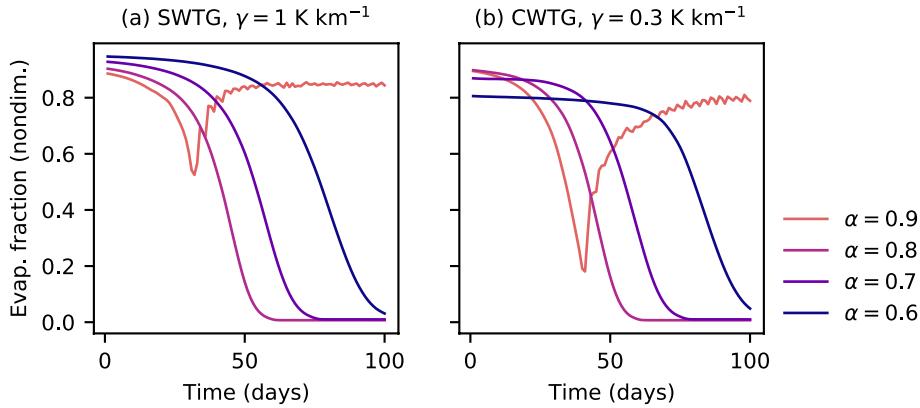

Figure 12. As in Figure 6a, but for simulations using the alternative spectral WTG (SWTG) scheme (a) and the conventional WTG (CWTG) scheme (b). Increases in evaporative fraction over time indicate transitions back to precipitating states.

surface dries out also looks somewhat different with the alternative SWTG and CWTG schemes: although transient increases in boundary layer MSE still occur, they are less dramatic than with the original SWTG scheme, and often appear because increases in boundary layer DSE outpace decreases in boundary layer moisture, not because both increase (Figure 13).

Overall, these results are consistent with our expectations. Alternative SWTG and CWTG simulations do retain key qualitative features of simulations with the original SWTG scheme: multiple equilibria still appear over an intermediate range of insolation, and surface drying is still capable of triggering a transition from a non-precipitating to a precipitating equilibrium. However, the escape from a dry equilibrium occurs less readily in alternative SWTG and CWTG simulations, emphasizing (as expected) that the robustness of dry equilibria in simulations with parameterized large-scale dynamics over a land surface is sensitive to how the parameterized circulation responds to changes in surface and boundary layer temperatures.

6. Conclusions

In this paper, we show that convection-permitting simulations support multiple equilibria in precipitation over a freely-evaporating land surface when coupled to a parameterization of large-scale circulations based on the WTG

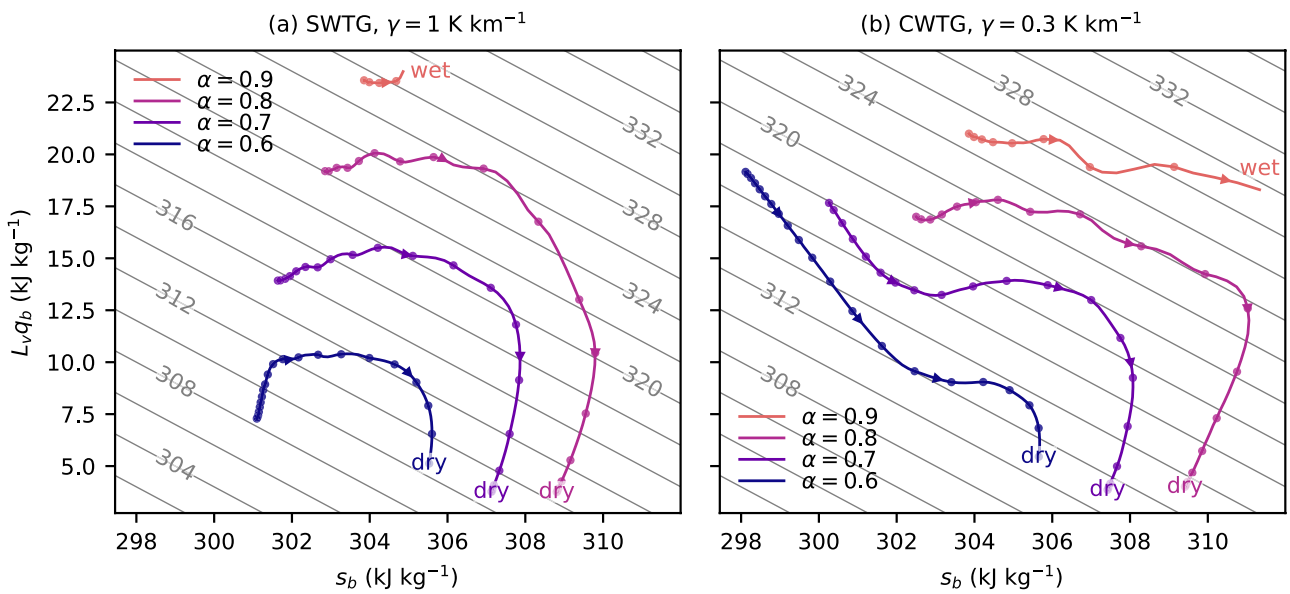

Figure 13. As in Figure 7a, but for simulations using the alternative spectral WTG (SWTG) scheme (a) and the conventional WTG (CWTG) scheme (b).

approximation (Section 3). The presence of multiple equilibria is fundamentally linked to interactive coupling between the model state and the parameterized large-scale circulation: this coupling produces an open hydrological cycle with a three-way balance between precipitation, evaporation, and large-scale moisture transport, permitting steady-states where precipitation balances evaporation and moisture convergence ("wet equilibria") and where moisture divergence balances evaporation ("dry equilibria"). We then demonstrate that a transient reduction in soil moisture, which increases sensible heat fluxes and decreases latent heat fluxes, can trigger a transition from a dry equilibrium back to a wet equilibrium (Section 4). This negative soil moisture-precipitation feedback is associated with an increase in boundary layer moisture that occurs despite reductions in evaporation, and that we link to increasingly inefficient boundary layer drying by the large-scale circulation. However, we also show that the degree of compensation between weaker moistening by evaporation and weaker drying by the large-scale circulation is sensitive to the formulation of the large-scale dynamics parameterization, and that modifying the large-scale dynamics parameterization can alter the parameter space where negative soil moisture-precipitation feedbacks occur (Section 5). We will conclude in this section with a discussion of the extent to which our results provide robust physical insight, and an outlook on the use of convection-permitting simulations with parameterized large-scale dynamics as a tool for process studies of land-atmosphere interactions.

Our first result—that multiple equilibria in precipitation are possible for a WTG-constrained atmosphere over a freely-evaporating land surface—seems likely to be a physically robust one. Although the parameter space where multiple equilibria appear is somewhat sensitive to the formulation of the WTG scheme (compare Figures 2 and 11), both precipitating and non-precipitating equilibria are supported over a fairly wide range of solar latitudes in all cases. Moreover, the existence of multiple equilibria in our WTG simulations is consistent with work on convective self-aggregation, a similar bifurcation into moist precipitating and dry non-precipitating regimes (Sentić & Sessions, 2017; Sessions et al., 2016). The freely evaporating land surface used in our fixed-soil-moisture simulations is essentially a thin slab ocean, and the small number of studies that examine self-aggregation in cloud-resolving simulations over an interactive surface suggest that coupling to a slab ocean delays but does not necessarily prevent the onset of convective self-aggregation (Hohenegger & Stevens, 2016; Shamekh et al., 2020; Tompkins & Semie, 2021) and may help maintain aggregated states once established (Shamekh et al., 2020). These results, which show that stable self-aggregated states are possible when coupled to a slab ocean, are echoed by ours, which show that large-amplitude moisture perturbations can lead to bifurcations into moist precipitating and dry non-precipitating equilibria in WTG simulations coupled to a freely-evaporating land surface. Exploring whether WPG (Edman & Romps, 2014; Kuang, 2008; Romps, 2012a) simulations exhibit multiple equilibria when coupled to a land-like surface is beyond the scope of this work, but is an interesting potential direction for future research. WPG simulations tend not to support multiple equilibria when coupled to a fixed-temperature ocean surface (Daleu et al., 2015), but the same is true of SWTG simulations (Herman & Raymond, 2014), and we nonetheless found robust bistability in SWTG simulations coupled to a land-like surface.

Our second result—that transient surface drying can trigger a transition from a non-precipitating state back to a precipitating state—seems physically plausible, but is less clearly robust. An increase in near-surface convergence and low-level ascent over a dry surface occurs in simulations with resolved soil moisture gradients (Hohenegger & Stevens, 2018; Imamovic et al., 2017; Taylor et al., 2013), which aligns with our finding that surface drying can reduce both evaporation and boundary layer ventilation by large-scale circulations, and suggests that including both effects of surface drying might be a useful refinement to simple models for the equilibrium boundary layer over land under the influence of fixed large-scale subsidence (Betts, 2000; Cronin, 2013; Kim & Entekhabi, 1998). Our sensitivity experiments highlight some reasons to be skeptical about how reliably WTG schemes simulate the link between surface drying, boundary layer temperature anomalies, and changes to the low-level large-scale circulation. Importantly, though, we do observe key qualitative similarities across sensitivity experiments with different WTG parameterizations: all exhibit bistability with fixed soil moisture, and all have at least one non-precipitating equilibrium where surface drying triggers a transition back to a precipitating state. Links between surface drying and low-level ascent are likely to be captured by WPG schemes, possibly more accurately than by WTG schemes, because WPG schemes directly parameterize the horizontal pressure gradients that drive low-level convergence over hot dry surfaces. This suggests that surface drying in simulations with WPG schemes may also favor the onset of precipitation, although confirming this prediction would require additional experiments that are outside the scope of this work.

Guillod et al. (2015) and Moon et al. (2019) argue that it can be insightful to distinguish between "spatial," "temporal," and heterogeneity-driven soil moisture-precipitation feedbacks. The negative soil moisture-precipitation

feedback identified in our simulations is similar to negative "spatial" feedbacks (rain more likely at locations where soil is dry) identified in previous studies (Guillod et al., 2015; Hohenegger & Stevens, 2018; Moon et al., 2019; Taylor et al., 2013) in that the feedback involves the onset of rain over an anomalously-dry surface. (In our simulations, the "anomaly" is felt through differences relative to the WTG reference temperature profile.) Notably, however, our simulations produce a negative feedback despite being unable to converge moisture released by evaporation from surrounding wet soil. The presence of multiple equilibria (i.e., persistent wet and dry states) in our WTG simulations suggests that observed positive "temporal" feedbacks (rain more likely during times when soil is wet) may be due at least in part to atmospheric persistence, as suggested by Guillod et al. (2015). The simulations reported here do not address heterogeneity-driven soil moisture-precipitation feedbacks (whether rain is more likely when soil moisture is more or less spatially heterogeneous). An early version of this work (Abbott, 2021) used simulations with spatially-varying surface properties to explore the influence of soil moisture heterogeneity on transitions from dry to wet equilibria, but we found robust results difficult to obtain because of sensitivity to poorly-resolved mixing in the nocturnal boundary layer.

Differences between our results with different WTG schemes can be traced back to uncertainties in how best to parameterize large-scale vertical motion near the surface. These uncertainties are weaknesses of WTG-constrained models of the land-atmosphere system, but they are counterbalanced by an important strength: parameterizing large-scale circulations provides a way to simulate a land region with an open hydrological cycle without running simulations on a large domain. For studies with convection-permitting models, this allows computational resources to be dedicated to increased resolution—important for accurately representing cloud-topped boundary layers, convective updraft speeds, free-tropospheric humidity, and mean cloud cover (Honnert et al., 2020; Jeevanjee, 2017; Jeevanjee & Zhou, 2022; Jenney et al., 2022)—or large parameter sweeps rather than increased domain size. Simulations with parameterized large-scale circulations also offer a simple tool for testing how physics parameterizations represent regional climate over tropical land, potentially providing a pathway to reducing the gap between soil moisture-precipitation feedbacks as represented with explicit versus parameterized convection (Hohenegger et al., 2009; Taylor et al., 2013).

So how best to move forward? One obvious need is some reasonable "ground truth" that can be used to validate (or invalidate) the response of WTG or WPG parameterizations to changes in land surface properties. One reasonable way to obtain this "ground truth" is by comparing simulations with explicitly simulated and parameterized large-scale circulations. This approach has been used in the past to test parameterizations of large-scale circulations over sea surface temperature "hotspots" (Romps, 2012a), and could be adapted to focus on the response to changes in land surface properties by replacing the "hotspot" with a patch of land, although some past studies (Cronin et al., 2015; Leutwyler & Hohenegger, 2021) highlight two-way interactions between islands and large-scale temperature profiles that may be difficult to capture in WTG or WPG simulations with fixed reference profiles. Additionally, introducing weak rotation in simulations with resolved large-scale circulations could provide a way to probe when WTG or WPG assumptions break down, a relevant question because regions where land-atmosphere coupling is strongest are somewhat off-equator (Dirmeyer, 2011), where the Coriolis parameter is small but non-zero. Alternatively, understanding how perturbations in surface fluxes at different scales project onto mesoscale circulations that converge or diverge moisture could be phrased as a problem in dry fluid dynamics, with a stable free troposphere overlying a neutrally-stratified boundary layer, imposed heterogeneity in surface buoyancy fluxes, and a moisture variable as a passive tracer. Solutions to this prototype problem could then be used as a test for local parameterizations of large-scale transports.

Ultimately, however, confidence in the fidelity of WTG parameterizations should be based on their ability to reproduce observations. To our knowledge, the only model-observation comparison for WTG simulations over land is the study of Anber, Gentine, et al. (2015), which provides compelling evidence that current versions of WTG parameterizations are capable of reproducing observations of Amazonian climate during both the wet and dry seasons. Their wet- and dry-season simulations both include substantial amounts of rainfall, and so build confidence in the ability of WTG-constrained models to represent precipitating states over tropical land. In contrast, our understanding of the behavior and fidelity of large-scale dynamics parameterizations in arid continental regimes—where strong heating can be confined to a relatively shallow boundary layer—is quite limited, and exploring the ability of WTG-constrained simulations to reproduce observed features of dry spells over tropical land would help develop a firmer foundation for their use across a broad range of climate states. Although this paper highlights some possible challenges in parameterizing the response of large-scale circulations to surface drying, it also documents rich behavior that can be leveraged to study how land-atmosphere coupling affects the

stability of wet and dry states, and so encourages an increased focus on the use of convection-permitting models with parameterized large-scale dynamics as idealized models for regional continental climate.

Data Availability Statement

SAM is publicly available (http://rossby.msrc.sunysb.edu/~marat/SAM.html). Modifications to the SAM source code, simulation input files, and simulation output underlying this work are archived at https://doi.org/10.5281/zenodo.8117628 (Abbott & Cronin, 2023).

Acknowledgments
The authors thank Marat Khairoutdinov for freely supplying SAM; Paul O'Gorman, David McGee, Larissa Back, and Sharon Sessions for feedback on an early version of this work; and Sarah Warnau and two anonymous reviewers for their helpful comments. This work was funded in part by the John W. Jarve (1978) Seed Fund for Science Innovation.

References

Abbott, T. H. (2021). Interactions between atmospheric deep convection and the surrounding environment (Doctoral dissertation) [Dataset]. Massachusetts Institute of Technology. Retrieved from https://dspace.mit.edu/handle/1721.1/139328

Abbott, T. H., & Cronin, T. W. (2023). Data for "multiple equilibria and soil moisture-precipitation feedbacks in idealized convection-permitting simulations with an open hydrological cycle" [Dataset]. Zenodo. https://doi.org/10.5281/zenodo.8117628

Anber, U., Gentine, P., Wang, S., & Sobel, A. H. (2015). Fog and rain in the amazon. *Proceedings of the National Academy of Sciences*, *112*(37), 11473–11477. https://doi.org/10.1073/pnas.1505077112

Anber, U., Wang, S., & Sobel, A. (2015). Effect of surface fluxes versus radiative heating on tropical deep convection. *Journal of the Atmospheric Sciences*, *72*(9), 3378–3388. https://doi.org/10.1175/jas-d-14-0253.1

Betts, A. K. (2000). Idealized model for equilibrium boundary layer over land. *Journal of Hydrometeorology*, *1*(6), 507–523. https://doi.org/10.1175/1525-7541(2000)001<0507:imfebl>2.0.co;2

Bretherton, C., & Blossey, P. (2017). Understanding mesoscale aggregation of shallow cumulus convection using large-eddy simulation. *Journal of Advances in Modeling Earth Systems*, *9*(8), 2798–2821. https://doi.org/10.1002/2017ms000981

Cioni, G., & Hohenegger, C. (2018). A simplified model of precipitation enhancement over a heterogeneous surface. *Hydrology and Earth System Sciences*, *22*(6), 3197–3212. https://doi.org/10.5194/hess-22-3197-2018

Cronin, T. W. (2013). A sensitivity theory for the equilibrium boundary layer over land. *Journal of Advances in Modeling Earth Systems*, *5*(4), 764–784. https://doi.org/10.1002/jame.20048

Cronin, T. W., & Emanuel, K. A. (2013). The climate time scale in the approach to radiative-convective equilibrium. *Journal of Advances in Modeling Earth Systems*, *5*(4), 843–849. https://doi.org/10.1002/jame.20049

Cronin, T. W., Emanuel, K. A., & Molnar, P. (2015). Island precipitation enhancement and the diurnal cycle in radiative-convective equilibrium. *Quarterly Journal of the Royal Meteorological Society*, *141*(689), 1017–1034. https://doi.org/10.1002/qj.2443

Daleu, C. L., Plant, R. S., Woolnough, S. J., Sessions, S., Herman, M. J., Sobel, A., et al. (2015). Intercomparison of methods of coupling between convection and large-scale circulation: 1. Comparison over uniform surface conditions. *Journal of Advances in Modeling Earth Systems*, *7*(4), 1576–1601. https://doi.org/10.1002/2015ms000468

Dirmeyer, P. A. (2011). The terrestrial segment of soil moisture–climate coupling. *Geophysical Research Letters*, *38*(16). https://doi.org/10.1029/2011gl048268

Doms, G., Förstner, J., Heise, E., Herzog, H.-J., Mironov, D., Raschendorfer, M., et al. (2011). *A description of the nonhydrostatic regional COSMO model part II: Physical parameterization*. Deutscher Wetterdienst.

Edman, J. P., & Romps, D. M. (2014). An improved weak pressure gradient scheme for single-column modeling. *Journal of the Atmospheric Sciences*, *71*(7), 2415–2429. https://doi.org/10.1175/jas-d-13-0327.1

Eltahir, E. A. (1998). A soil moisture–rainfall feedback mechanism: 1. Theory and observations. *Water Resources Research*, *34*(4), 765–776. https://doi.org/10.1029/97wr03499

Findell, K. L., & Eltahir, E. A. (2003). Atmospheric controls on soil moisture–boundary layer interactions. Part I: Framework development. *Journal of Hydrometeorology*, *4*(3), 552–569. https://doi.org/10.1175/1525-7541(2003)004<0552:acosml>2.0.co;2

Froidevaux, P., Schlemmer, L., Schmidli, J., Langhans, W., & Schär, C. (2014). Influence of the background wind on the local soil moisture–precipitation feedback. *Journal of the Atmospheric Sciences*, *71*(2), 782–799. https://doi.org/10.1175/jas-d-13-0180.1

Guillod, B. P., Orlowsky, B., Miralles, D. G., Teuling, A. J., & Seneviratne, S. I. (2015). Reconciling spatial and temporal soil moisture effects on afternoon rainfall. *Nature Communications*, *6*(1), 6443. https://doi.org/10.1038/ncomms7443

Herman, M. J., & Raymond, D. J. (2014). WTG cloud modeling with spectral decomposition of heating. *Journal of Advances in Modeling Earth Systems*, *6*(4), 1121–1140. https://doi.org/10.1002/2014ms000359

Hohenegger, C., Brockhaus, P., Bretherton, C. S., & Schär, C. (2009). The soil moisture–precipitation feedback in simulations with explicit and parameterized convection. *Journal of Climate*, *22*(19), 5003–5020. https://doi.org/10.1175/2009jcli2604.1

Hohenegger, C., & Stevens, B. (2016). Coupled radiative convective equilibrium simulations with explicit and parameterized convection. *Journal of Advances in Modeling Earth Systems*, *8*(3), 1468–1482. https://doi.org/10.1002/2016ms000666

Hohenegger, C., & Stevens, B. (2018). The role of the permanent wilting point in controlling the spatial distribution of precipitation. *Proceedings of the National Academy of Sciences*, *115*(22), 5692–5697. https://doi.org/10.1073/pnas.1718842115

Honnert, R., Efstathiou, G. A., Beare, R. J., Ito, J., Lock, A., Neggers, R., et al. (2020). The atmospheric boundary layer and the "gray zone" of turbulence: A critical review. *Journal of Geophysical Research: Atmospheres*, *125*(13), 1–26. https://doi.org/10.1029/2019jd030317

Imamovic, A., Schlemmer, L., & Schär, C. (2017). Collective impacts of orography and soil moisture on the soil moisture-precipitation feedback. *Geophysical Research Letters*, *44*(22), 11–682. https://doi.org/10.1002/2017gl075657

Jeevanjee, N. (2017). Vertical velocity in the gray zone. *Journal of Advances in Modeling Earth Systems*, *9*(6), 2304–2316. https://doi.org/10.1002/2017ms001059

Jeevanjee, N., & Zhou, L. (2022). On the resolution-dependence of anvil cloud fraction and precipitation efficiency in radiative-convective equilibrium. *Journal of Advances in Modeling Earth Systems*, *14*(3), 1–17. https://doi.org/10.1029/2021ms002759

Jenney, A. M., Ferretti, S. L., & Pritchard, M. S. (2022). Vertical resolution impacts explicit simulation of deep convection. *ESS Open Archive*, 1–26. https://doi.org/10.1002/essoar.10512579.1

Khairoutdinov, M. F., & Randall, D. A. (2003). Cloud resolving modeling of the ARM summer 1997 IOP: Model formulation, results, uncertainties, and sensitivities. *Journal of the Atmospheric Sciences*, *60*(4), 607–625. https://doi.org/10.1175/1520-0469(2003)060<0607:crmota>2.0.co;2

Kim, C., & Entekhabi, D. (1998). Feedbacks in the land-surface and mixed-layer energy budgets. *Boundary-Layer Meteorology*, *88*(1), 1–21. https://doi.org/10.1023/a:1001094008513

Kuang, Z. (2008). Modeling the interaction between cumulus convection and linear gravity waves using a limited-domain cloud system–resolving model. *Journal of the Atmospheric Sciences*, *65*(2), 576–591. https://doi.org/10.1175/2007jas2399.1

Leutwyler, D., & Hohenegger, C. (2021). Weak cooling of the troposphere by tropical islands in simulations of the radiative-convective equilibrium. *Quarterly Journal of the Royal Meteorological Society*, *147*(736), 1788–1800. https://doi.org/10.1002/qj.3995

Leutwyler, D., Imamovic, A., & Schär, C. (2021). The continental-scale soil moisture–precipitation feedback in Europe with parameterized and explicit convection. *Journal of Climate*, *34*(13), 5303–5320. https://doi.org/10.1175/jcli-d-20-0415.1

Mlawer, E. J., Taubman, S. J., Brown, P. D., Iacono, M. J., & Clough, S. A. (1997). Radiative transfer for inhomogeneous atmospheres: RRTM, a validated correlated-k model for the longwave. *Journal of Geophysical Research*, *102*(D14), 16663–16682. https://doi.org/10.1029/97jd00237

Moon, H., Guillod, B. P., Gudmundsson, L., & Seneviratne, S. I. (2019). Soil moisture effects on afternoon precipitation occurrence in current climate models. *Geophysical Research Letters*, *46*(3), 1861–1869. https://doi.org/10.1029/2018gl080879

Naumann, A. K., Stevens, B., & Hohenegger, C. (2019). A moist conceptual model for the boundary layer structure and radiatively driven shallow circulations in the trades. *Journal of the Atmospheric Sciences*, *76*(5), 1289–1306. https://doi.org/10.1175/jas-d-18-0226.1

Raymond, D. J., Sessions, S. L., Sobel, A. H., & Fuchs, Ž. (2009). The mechanics of gross moist stability. *Journal of Advances in Modeling Earth Systems*, *1*(3), 1–20. https://doi.org/10.3894/james.2009.1.9

Raymond, D. J., & Zeng, X. (2005). Modelling tropical atmospheric convection in the context of the weak temperature gradient approximation. *Quarterly Journal of the Royal Meteorological Society*, *131*(608), 1301–1320. https://doi.org/10.1256/qj.03.97

Rieck, M., Hohenegger, C., & van Heerwaarden, C. C. (2014). The influence of land surface heterogeneities on cloud size development. *Monthly Weather Review*, *142*(10), 3830–3846. https://doi.org/10.1175/mwr-d-13-00354.1

Romps, D. M. (2012a). Numerical tests of the weak pressure gradient approximation. *Journal of the Atmospheric Sciences*, *69*(9), 2846–2856. https://doi.org/10.1175/jas-d-11-0337.1

Romps, D. M. (2012b). Weak pressure gradient approximation and its analytical solutions. *Journal of the Atmospheric Sciences*, *69*(9), 2835–2845. https://doi.org/10.1175/jas-d-11-0336.1

Romps, D. M. (2020). Climate sensitivity and the direct effect of carbon dioxide in a limited-area cloud-resolving model. *Journal of Climate*, *33*(9), 3413–3429. https://doi.org/10.1175/jcli-d-19-0682.1

Ross, C. W., Prihodko, L., Anchang, J., Kumar, S., Ji, W., & Hanan, N. P. (2018). Hysogs250m, global gridded hydrologic soil groups for curve-number-based runoff modeling. *Scientific Data*, *5*(1), 1–9. https://doi.org/10.1038/sdata.2018.91

Sentić, S., & Sessions, S. L. (2017). Idealized modeling of convective organization with changing sea surface temperatures using multiple equilibria in weak temperature gradient simulations. *Journal of Advances in Modeling Earth Systems*, *9*(2), 1431–1449. https://doi.org/10.1002/2016ms000873

Sessions, S. L., Herman, M. J., & Sentić, S. (2015). Convective response to changes in the thermodynamic environment in idealized weak temperature gradient simulations. *Journal of Advances in Modeling Earth Systems*, *7*(2), 712–738. https://doi.org/10.1002/2015ms000446

Sessions, S. L., Sentić, S., & Herman, M. J. (2016). The role of radiation in organizing convection in weak temperature gradient simulations. *Journal of Advances in Modeling Earth Systems*, *8*(1), 244–271. https://doi.org/10.1002/2015ms000587

Sessions, S. L., Sugaya, S., Raymond, D. J., & Sobel, A. H. (2010). Multiple equilibria in a cloud-resolving model using the weak temperature gradient approximation. *Journal of Geophysical Research*, *115*(D12), 1–17. https://doi.org/10.1029/2009jd013376

Shamekh, S., Muller, C., Duvel, J.-P., & d'Andrea, F. (2020). Self-aggregation of convective clouds with interactive sea surface temperature. *Journal of Advances in Modeling Earth Systems*, *12*(11), 1–21. https://doi.org/10.1029/2020ms002164

Sobel, A. H., Bellon, G., & Bacmeister, J. (2007). Multiple equilibria in a single-column model of the tropical atmosphere. *Geophysical Research Letters*, *34*(22), 1–5. https://doi.org/10.1029/2007gl031320

Sobel, A. H., & Bretherton, C. S. (2000). Modeling tropical precipitation in a single column. *Journal of Climate*, *13*(24), 4378–4392. https://doi.org/10.1175/1520-0442(2000)013<4378:mtpias>2.0.co;2

Sobel, A. H., Nilsson, J., & Polvani, L. M. (2001). The weak temperature gradient approximation and balanced tropical moisture waves. *Journal of the Atmospheric Sciences*, *58*(23), 3650–3665. https://doi.org/10.1175/1520-0469(2001)058<3650:twtgaa>2.0.co;2

Taylor, C. M., Birch, C. E., Parker, D. J., Dixon, N., Guichard, F., Nikulin, G., & Lister, G. M. (2013). Modeling soil moisture-precipitation feedback in the Sahel: Importance of spatial scale versus convective parameterization. *Geophysical Research Letters*, *40*(23), 6213–6218. https://doi.org/10.1002/2013gl058511

Taylor, C. M., de Jeu, R. A., Guichard, F., Harris, P. P., & Dorigo, W. A. (2012). Afternoon rain more likely over drier soils. *Nature*, *489*(7416), 423–426. https://doi.org/10.1038/nature11377

Tompkins, A. M., & Semie, A. G. (2021). Impact of a mixed ocean layer and the diurnal cycle on convective aggregation. *Journal of Advances in Modeling Earth Systems*, *13*(12), 1–29. https://doi.org/10.1029/2020ms002186

Trenberth, K. E. (1999). Atmospheric moisture recycling: Role of advection and local evaporation. *Journal of Climate*, *12*(5), 1368–1381. https://doi.org/10.1175/1520-0442(1999)012<1368:amrroa>2.0.co;2

Wang, S., & Sobel, A. H. (2011). Response of convection to relative sea surface temperature: Cloud-resolving simulations in two and three dimensions. *Journal of Geophysical Research*, *116*(D11), 1–19. https://doi.org/10.1029/2010jd015347

Wing, A. A., Reed, K. A., Satoh, M., Stevens, B., Bony, S., & Ohno, T. (2018). Radiative–convective equilibrium model intercomparison project. *Geoscientific Model Development*, *11*(2), 793–813. https://doi.org/10.5194/gmd-11-793-2018

Zhang, Y., & Fueglistaler, S. (2020). How tropical convection couples high moist static energy over land and ocean. *Geophysical Research Letters*, *47*(2), 1–8. https://doi.org/10.1029/2019gl086387